Kinetics of the IO Radical. 2. Reaction of IO with BrO

Mary K. Gilles, Andrew A. Turnipseed,† James B. Burkholder, A. R. Ravishankara,* and Susan Solomon

Aeronomy Laboratory, National Oceanic and Atmospheric Administration, Boulder, Colorado 80303, and Cooperative Institute for Research in Environmental Sciences, University of Colorado, Boulder, Colorado 80309

Received: March 12, 1997; In Final Form: May 9, 1997[⊗]

The rate coefficient for the IO + BrO → products (1) reaction was measured using pulsed laser photolysis with a discharge flow tube for radical production and pulsed laser-induced fluorescence and UV absorption for detection of IO and BrO radicals, respectively. Reaction 1 was studied under pseudo-first-order conditions in IO with an excess of BrO between 204 and 388 K at total pressures of 6−15 Torr. The Arrhenius expression obtained for non-iodine atom producing channels is $k_{1a}(T) = (2.5 \pm 1.0) \times 10^{-11} \exp[(260 \pm 100)/T]$ cm^3 molecule^{-1} s^{-1} independent of pressure. The rate coefficient for the reaction BrO + BrO → products (2) and the UV absorption cross sections of BrO as a function of temperature were also determined as part of this study. The implications of these results to the loss rate of stratospheric ozone are discussed.

Introduction

In the preceding paper,[1] we described the role of iodine chemistry in the lower stratosphere and marine boundary layer and its potential contribution to the observed low-altitude ozone depletion in the extrapolar regions. Enhanced levels of BrO and IO have been measured (BrO) or suspected (IO) in the Arctic winter/spring lower troposphere, where ozone depletion episodes have been observed.[2] The reactions of IO + BrO (1) and BrO + BrO (2) play an important role in interpreting this ozone depletion because both iodine and bromine can be rapidly released into the atmosphere from their source gases or sea salt particles.

In this paper we report rate coefficient measurements for the reactions

$$\mathrm{IO + BrO \rightarrow products\ (non\text{-}iodine\ atom\ producing\ channels)} \quad (1a)$$

$$\rightarrow \mathrm{I + products} \quad (1b)$$

where $k_1 = k_{1a} + k_{1b}$, and

$$\mathrm{BrO + BrO \rightarrow products} \quad (2)$$

as functions of temperature. Supplementary to these studies we also report BrO UV absorption cross sections over the same temperature range and model calculations on the atmospheric implications of the IO + BrO and IO + ClO reactions.

Experimental Section

The experiments described in this paper were carried out on two different apparatus. The first part of this section details the measurement of the BrO absorption cross sections and the BrO self-reaction. The second part pertains to the generation and detection of IO and BrO for the determination of k_1.

BrO Absorption Cross Sections. *BrO Absolute Absorption Cross Sections.* The absolute absorption cross section of the (7,0) band in the $A^2\Pi_{3/2} \leftarrow X^2\Pi_{3/2}$ transition of BrO was determined using transient UV absorption following pulsed photolysis of N_2O/O_2 and N_2O/Br_2 mixtures. The apparatus has been described in previous papers.[3,4] The apparatus consists of a temperature-controlled absorption cell (87 cm long), a pulsed photolysis laser (193 nm, ArF excimer laser), and a UV probe light source (cw 75 W Xe lamp) combined with a 0.25 m monochromator/photomultiplier (PMT) detector.

The photolysis laser beam (0.1 Hz) was copropagated through the absorption cell with the probe beam. The probe beam, upon exiting the cell, was directed onto the entrance slit of the monochromator tuned to either the peak of the (7,0) transition of BrO (∼338 nm) or the O_3 absorption (253.7 nm). The output of the PMT was offset by a DC bias, and the difference was amplified and fed to a signal averager that was pretriggered to acquire the light intensity prior to the laser pulse. BrO was generated following the pulse (see below), and the light intensity was recorded as a function of time. The monochromator resolution, 0.5 nm (fwhm), was set by adjusting the slit width while monitoring the 253.7 nm emission from a mercury pen ray lamp.

In a series of back-to-back experiments, while keeping $[N_2O]$ and the laser fluence constant, BrO and O_3 were produced from $O(^3P)$ reactions. $O(^3P)$ was produced via 193 nm photolysis[5] of N_2O in N_2 (500−550 Torr):

$$\mathrm{N_2O} + h\nu \rightarrow \mathrm{N_2} + \mathrm{O(^1D)} \quad (3)$$

$$\mathrm{O(^1D) + N_2 \rightarrow O(^3P) + N_2} \quad (4)$$

Br_2 was added to the cell to produce BrO via the reaction[6]

$$\mathrm{O(^3P) + Br_2 \rightarrow BrO + Br} \quad (5)$$

BrO formation was essentially instantaneous on the time scale of BrO loss. Then Br_2 was removed from the cell and O_2 (20−30 Torr) was added. The temporal profile of O_3 formed in the reaction

$$\mathrm{O(^3P) + O_2 + M \rightarrow O_3 + M} \quad (6)$$

* Address correspondence to this author at: NOAA/ERL, R/E/AL2, 325 Broadway, Boulder, CO 80303. Email: Ravi@al.noaa.gov. Also affiliated with the Department of Chemistry and Biochemistry, University of Colorado, Boulder, CO 80309.

† Current address: Department of Biology (EPOB), University of Colorado, Boulder, CO 80309.

⊗ Abstract published in *Advance ACS Abstracts,* July 1, 1997.

S1089-5639(97)00915-8 CCC: $14.00

was measured. O_3 produced from O_2 photolysis in the cell and in the beam path external to the cell (2−10% of that produced with N_2O in the cell) was measured without N_2O in the cell and subtracted. BrO profiles were analyzed for second-order loss of BrO, reaction 2, and extrapolated to time zero to obtain A_0^{BrO}, the absorption due to the initial BrO production. O_3 absorbance profiles also showed a rapid rise to an asymptotic value. Absorbance values measured at long times were averaged to obtain A^{O_3}, the absorption due to O_3 production. The concentration of O_3 and BrO formed are equal to the initial concentration of $O(^3P)$ atoms produced, and the absorption cross section of the (7,0) band of BrO (σ^{BrO}) is given by

$$\sigma^{BrO} = \frac{A_0^{BrO}}{A^{O_3}} \sigma^{O_3}_{253.7nm} \qquad \text{(I)}$$

where $\sigma^{O_3}_{253.7nm}$ is the absorption cross section of O_3 at 253.7 nm. The analysis of the BrO temporal profiles also yielded the ratio $2k_2/(\sigma^{BrO}l)$, which when combined with the BrO absorption cross section yields k_2. σ^{BrO} and k_2 were determined at nine temperatures between 204 and 388 K.

Reaction of IO + BrO. The apparatus used to study reaction 1 was described in the previous paper.[1] Therefore, only the modifications for this study are described here. k_1 was measured under pseudo-first-order conditions with BrO in excess. BrO was generated in a discharge flow system and passed into the reactor, which doubled as the absorption cell, where [BrO] was quantified by UV absorption. IO was produced by pulsed laser photolysis in the reactor, and its temporal profile was monitored by pulsed LIF.[7] Because BrO is more reactive than ClO, contributions from secondary chemistry are more problematic and need to be addressed to determine k_1.

BrO Source for Reaction 1. BrO was produced in a Pyrex flow tube (2.54 cm i.d. and 28 cm long) with a Teflon insert to minimize the loss of free radicals on the wall. A dilute mixture of Br_2 in He was passed through a microwave discharge located on a side arm of the flow tube. Ozone was added to the flow tube via a movable injector (0.6 cm o.d.). The tip of the movable injector was positioned downstream of the Br atom port. BrO was produced via the reaction[5]

$$Br + O_3 \rightarrow BrO + O_2 \qquad (7)$$

This BrO source was preferred, over reaction 5 for example, because the O_3 will scavenge any Br atoms produced in reaction 2. Typically, flow rates of 17−34 cm^3 s^{-1} (at 6−15 Torr) of a mixture of N_2 (∼10%) and He (∼90%) were used with linear gas flow velocities of 500−900 cm s^{-1}. The residence time of the gas in the reactor was 40−80 ms. The concentration of BrO was varied from (1 to 25) × 10^{12} molecule cm^{-3}, and the concentration of ozone in the reactor was (3−20) × 10^{14} molecule cm^{-3}. Because k_7 decreases with temperature {$k_7(T) = 1.7 \times 10^{-11}$ exp[−(800 ± 200)/T] cm^3 molecule^{-1} s^{-1}}[5] the concentration of O_3 was increased at lower temperatures to recycle Br atoms efficiently.

Measurement of [BrO] in Determining k_1. Absorption spectra were recorded over the wavelength range between 220 and 385 nm with a diode array spectrometer. This range allowed simultaneous measurement of both O_3 and BrO. As shown in Figure 1a, Br_2 and CF_3I also absorb in this region. Table 1 lists the absorption cross sections used to determine concentrations of these species.

The determination of [BrO] involved two steps: (i) first the light intensity (I_0) was measured with O_3 and Br_2 flowing through absorption cell, and (ii) the discharge source was turned on and the light intensity (I) was recorded. The absorption spectrum was determined using the relation $A = \ln(I_0/I) = n\sigma l$, where n was the concentration, σ was the differential absorption cross section, and l was the path length. An example of a measurement is shown in Figure 1b (lower trace). The negative ozone absorption is due to the loss of ozone via reaction 7. Due to recycling of Br atoms produced in the BrO self-reaction, there is not a one-to-one correspondence between O_3 lost and BrO formed. Adding back part of the O_3 absorption, using a reference spectrum, yields the upper trace in Figure 1b (offset from zero for clarity) attributed to only BrO. Although [Br_2] changes slightly, it is not measurable due to the small Br_2 cross section in this wavelength region. To minimize effects due to base line shifts, differential cross sections were used to calculate [BrO]. Reference BrO absorption spectra over the range 240−380 nm were measured with the diode array spectrometer with a 0.5 nm (fwhm) resolution at each temperature. These spectra were placed on an absolute scale using the absolute cross section measured for the (7,0) band, and the differential absorption cross section was calculated.

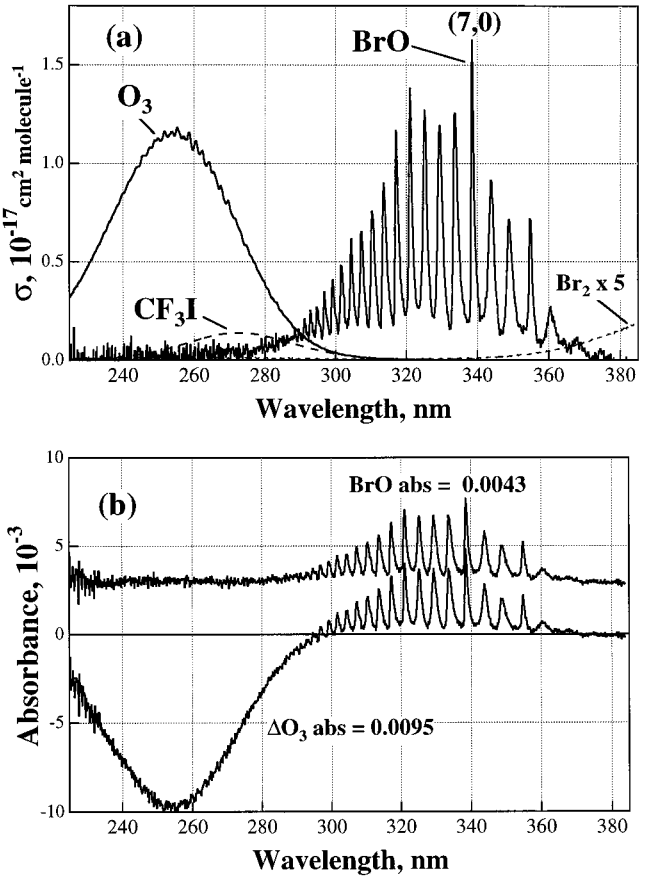

Figure 1. (a) UV reference absorption spectra of O_3, BrO, and Br_2. (b) Lower trace is a BrO spectrum measured before subtracting a reference ozone spectrum. The upper trace (offset from zero for clarity) is the BrO spectrum with O_3 subtracted.

TABLE 1: Absorption Cross Sections Used in These Experiments

species	λ (nm)	σ^a	ref
CF_3I	266	6.44	26
	193	<0.1	*b*
O_3	253.7	116	27
	193	4.33	27
Br_2	370	1.82	28
N_2O	193	0.895	5

[a] Units for σ are 10^{-19} cm^2 molecule^{-1}. [b] Estimated from ref 26.

The absorption cross section of BrO is temperature dependent, and an accurate determination of [BrO] requires a constant temperature over the entire absorption path. Therefore, the entire reactor was cooled, and the temperature gradient along the length of the reactor was measured. The cell windows were inset into the reactor at positions where the temperature was constant along the length of the cell. This is the primary difference in the apparatus used here and that used in the ClO experiment[1] where only a portion of the cell was cooled to reduce Cl_2O_2 formation. The temperature at the intersection point of the photolysis and probe lasers was measured by inserting a calibrated thermocouple through a movable injector under flow conditions identical to those used in measuring k_1. He (<5% of the total flow) was injected in front of the reactor windows through which the photolysis beam entered to prevent formation of deposits on the windows. The flush gas slightly changed both the composition at the extreme ends of the absorption cell and the path length for measuring absorbance of BrO. To determine the effective path length, CF_3I was flowed through the cell and the absorbance at 253.7 nm was measured with the diode array spectrometer. Using the known cross sections and the CF_3I concentration (calculated from measured flow rates), the effective path length was determined to be 36.6 ± 0.4 cm, <1% shorter than the physical length of the cell (37 cm).

IO Production. IO was produced via the 193 nm photolysis of an O_3/CF_3I mixture in the reactor. The photolysis laser beam passed through the cell counter to the direction of the gas flow. $O(^1D)$ produced by photolysis of O_3 was quickly quenched[5] to $O(^3P)$ by N_2; $O(^3P)$ reacted with CF_3I to produce IO.[8] O_3 was added with the main He/N_2 flow and CF_3I $\{(8-24) \times 10^{14}$ molecule $cm^{-3}\}$ directly to the reactor. The initial concentration of IO was kept below 2×10^{11} molecule cm^{-3} by using $<(0.1-0.75)$ mJ $pulse^{-1}$ cm^{-2} of 193 nm laser fluence with $(3-20) \times 10^{14}$ molecule cm^{-3} of O_3. CF_3I photolysis was an insignificant source of IO. The IO decay rates measured in the absence of BrO, with varying photolysis laser fluence, showed that IO loss was determined by flow out of the detection zone and not by its self-reaction.

Materials. N_2 (UHP, >99.9999%) and He (UHP, 99.9999%), N_2O (electronic grade), and CF_3I (99%) were used as supplied, and their flow rates were measured using calibrated electronic flow meters. The concentrations of N_2O and CF_3I were calculated from flows, and the total pressure was measured by a 100 Torr capacitance manometer. The CF_3I concentration was verified by UV/visible absorption. A dilute mixture of Br_2 in He was made by passing He through a trap containing Br_2 (99%), which was used without purification. The concentration of BrO was varied by changing the flow of He and/or the temperature (208−238 K) of the Br_2 trap. O_3 was produced by passing O_2 (UHP) through an ozonizer and trapping it on silica gel at 195 K. Ozone was added to the flow tube by passing a small flow of He through the silica gel trap, and its concentration was measured by UV/visible absorption at 253.7 nm.

Results

BrO Absorption Cross Sections as a Function of Temperature. BrO and O_3 temporal profiles obtained using the monochromator/PMT combination in back-to-back experiments are shown in Figure 2. Although there is no obvious change in the width of the vibronic bands, the BrO absolute absorption cross sections increase linearly with decreasing temperature and are described well by $\sigma^{BrO}(T) = 3.29-(5.58 \times 10^{-3}) \times (T)$ in units of 10^{-17} cm^2 $molecule^{-1}$ where the temperature is in kelvin. The absolute and differential absorption cross sections obtained at nine temperatures are given in Table 2.

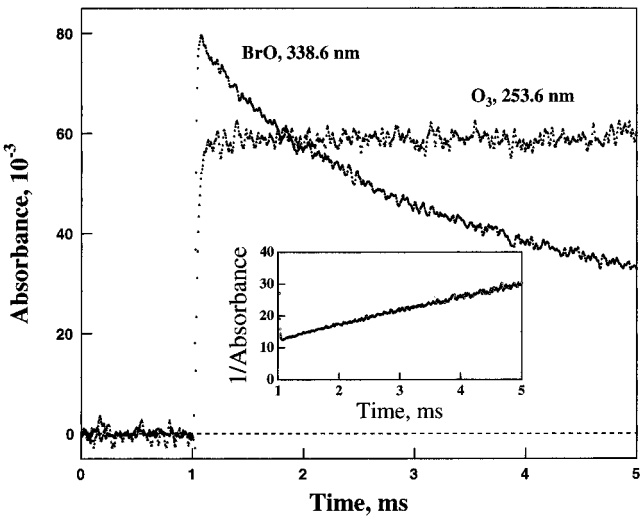

Figure 2. Temporal profiles of the BrO absorption measured at the peak of the (7,0) band and O_3 (253.6 nm) taken at 220 K. These profiles were used to calculate the BrO absolute absorption cross section at temperatures from 204 to 388 K with a spectral resolution of 0.5 nm. The insert is a second-order plot of $1/A_0^{BrO}$ vs time.

TABLE 2: BrO Absorption Cross Sections Measured as a Function of Temperature

T (K)	absolute[a]	differential[b]
388	1.12	0.94
369	1.23	1.01
329	1.45	1.22
298	1.63	1.44
273	1.84	1.66
252	1.88	1.68
237	1.97	1.67
222	2.05	1.83
204	2.15	1.93

[a] Absolute absorption cross section (units of 10^{-17} cm^2 $molecule^{-1}$) determined at the peak of the (7,0) band of the ($A^2\Pi_{3/2} \leftarrow X^2\Pi_{3/2}$) BrO transition at ~338 nm measured with a resolution of 0.5 nm (fwhm). [b] Differential cross section between the (7,0) band and the valley at shorter wavelength. Units are in 10^{-17} cm^2 $molecule^{-1}$.

BrO + BrO Reaction Rate Coefficients. Temporal profiles of BrO were measured in (1−5) Torr of N_2O, with $\sim 9 \times 10^{14}$ molecule cm^{-3} of Br_2 and ~500 Torr of N_2. The concentration of Br_2 was estimated from the rise time for BrO. It was assumed that the loss of $O(^3P)$ was due solely to reaction 5, $k_5 = 1.4 \times 10^{-11}$ cm^3 $molecule^{-1}$ s^{-1},[9] and that N_2O, N_2, and Br_2 do not react with BrO. The loss rate of BrO due to

$$BrO + BrO \rightarrow 2\,Br + O_2 \quad (2a)$$

$$\rightarrow Br_2 + O_2 \quad (2b)$$

is given by

$$\frac{d[BrO]}{dt} = -2k_2[BrO]^2 \quad (II)$$

Integration of eq II yields

$$\frac{1}{[BrO]_t} = \frac{1}{[BrO]_0} + 2k_2t \quad (III)$$

which, when expressed in terms of the measured absorbances, leads to

$$\frac{1}{A_t^{BrO}} = \frac{1}{A_0^{BrO}} + \frac{2k_2t}{\sigma^{BrO}l} \quad \text{(IV)}$$

Here A_t^{BrO} is the BrO absorption at time t, k_2 is the rate coefficient for reaction 2, σ^{BrO} is the BrO absolute absorption cross section, and l is the length of the absorption cell (87 cm). A plot of $1/A_t^{BrO}$ vs reaction time was linear with a slope of $2k_2/(\sigma^{BrO}l)$ and an intercept of $1/A_0^{BrO}$ (Figure 2, inset). Using the cross sections determined above, k_2 was calculated from the measured slopes. The rate coefficients are given in Table 3 and plotted in the Arrhenius form in Figure 3 (filled circles). Our results are well represented by the expression $k_2(T) = (1.70 \pm 0.45) \times 10^{-12} \exp[(215 \pm 50)/T]$ cm^3 molecule^{-1} s^{-1}. This expression was obtained from a weighted ($1/\sigma^2$) least-squares fit to a linearized form (ln k_2 vs $1/T$) of the Arrhenius expression. The quoted uncertainty includes 2σ precision from the fit plus 20% uncertainty for estimated systematic errors and the uncertainty in the BrO absorption cross section (10%).

BrO + IO Reaction Rate Coefficients. Reactions influencing the rise of the IO concentration were

$$O_3 + h\nu \rightarrow O_2 + O(^1D) \quad (8)$$

$$O(^1D) + N_2 \rightarrow O(^3P) + N_2 \quad (4)$$

$$O(^3P) + CF_3I \rightarrow CF_3 + IO \quad (9a)$$

$$\rightarrow \text{products other than IO} \quad (9b)$$

$$O(^3P) \rightarrow \text{loss} \quad (10)$$

$$O(^3P) + Br_2 \rightarrow BrO + Br \quad (5)$$

$$O(^3P) + BrO \rightarrow Br + O_2 \quad (11)$$

Quenching of $O(^1D)$ by N_2 is rapid[5] on the time scale of the subsequent chemistry. Reaction 9 produces IO with a yield >80%.[8] Sufficient CF_3I {$(8-24) \times 10^{14}$ molecule cm^{-3}} was present for IO formation to be complete in <200 μs. $O(^3P)$ atoms were lost via reactions 9, 5, and 11. Whenever [BrO] was varied, the concentration of CF_3I was adjusted to maintain approximately the same maximum IO signal. Since $[O(^3P)]_0 \ll [BrO]_0$, any contribution to the BrO concentration from reaction 5 was insignificant compared to the total [BrO].

The decay of the IO signal was controlled by the reactions

$$IO + BrO \rightarrow \text{products (non-iodine atom producing channels)} \quad (1a)$$

$$\rightarrow I + \text{products} \quad (1b)$$

$$IO \rightarrow \text{loss} \quad (12)$$

In the presence of a large concentration of O_3, I atoms are recycled to IO by the reaction:

$$I + O_3 \rightarrow IO + O_2 \quad (13)$$

where $K_{13}(T) = 2.3 \times 10^{-11} \exp[-860/T]$ cm^3 molecule^{-1} s^{-1},[7] making these measurements insensitive to channel 1b. Temporal profiles of IO measured at various BrO concentrations, in excess O_3, are shown in Figure 4 and are described by the expression:

$$[IO]_t = \frac{k_{9a}[O][CF_3I]}{k'_d - k'_a}(e^{-k'_a t} - e^{-k'_d t}) \quad \text{(V)}$$

TABLE 3: Results for k_2, Determined in This Experiment[a]

T (K)	k_2	number of measurements
388	2.77 ± 0.16	3
368	2.99 ± 0.30	5
331	3.21 ± 0.10	3
298	3.51 ± 0.35	6
273	3.91 ± 0.13	4
252	3.86 ± 0.27	2
237	4.04 ± 0.12	4
222	4.25 ± 0.45	4
204	4.83 ± 0.48	6

[a] Units for the rate coefficient are 10^{-12} cm^3 molecule^{-1} s^{-1}, and the uncertainty given is 2σ from the fit.

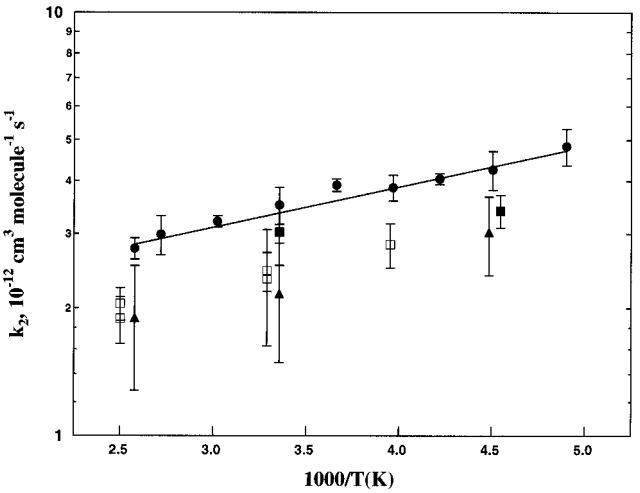

Figure 3. Arrhenius plot of k_2 vs 1000/T(K) (this work: filled circles), yielding the expression $k_2(T) = (1.70 \pm 0.45) \times 10^{-12} \exp[(215 \pm 50)/T]$ cm^3 molecule^{-1} s^{-1}. The results from Mauldin *et al.*[3] (■) are scaled to our BrO cross sections, while those of Sander *et al.*[14] (▲) and Turnipseed *et al.*[17] (□), are those quoted by the authors.

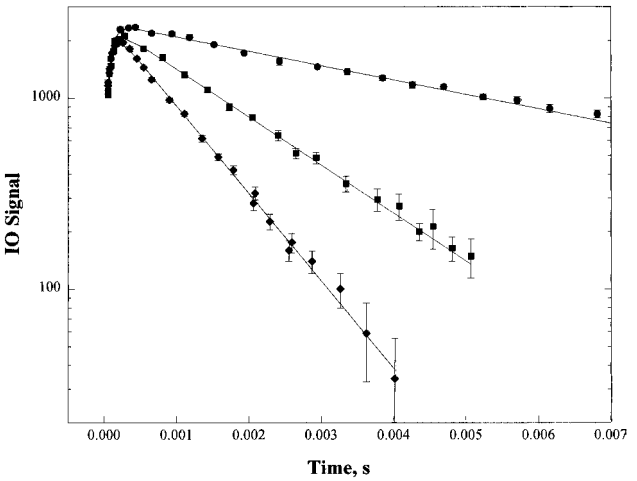

Figure 4. Plot of IO signal from laser-induced fluorescence as a function of BrO concentration (filled circles were measured with [BrO] = 0, filled squares with [BrO] = 6.77×10^{12} molecule cm^{-3}, and filled diamonds with [BrO] =14.4×10^{12} molecule cm^{-3}). The solid lines are fits to eq V.

where $k'_d = k_{1a}[BrO] + k_{12}$ and $k'_a = k_9[CF_3I] + k_{11}[BrO] + k_5[Br_2] + k_{10}$. Because the loss of IO was 20−30 times slower than its rise, usually only the decay of IO was measured and fit to the equation

$$[IO]_t = [IO]_0 e^{-k'_d t} \quad \text{(VI)}$$

to obtain k'_d. Values of k_{1a} determined using eqs V and VI were

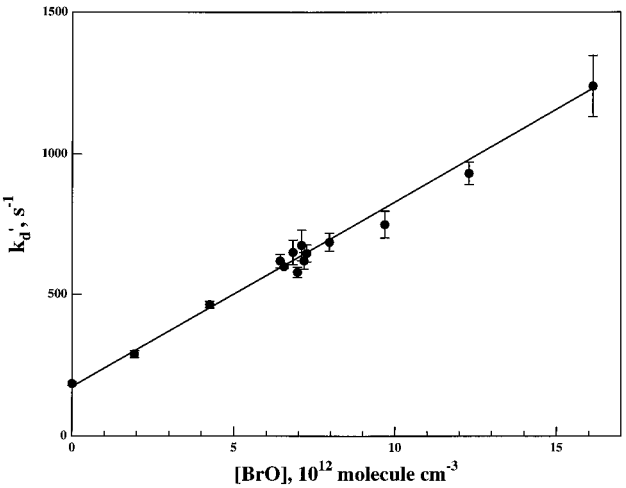

Figure 5. Pseudo-first-order rate coefficient, k'_d, as a function of BrO concentration at 298 K. The slope yielded the first-order reaction rate coefficient of $(6.07 \pm 0.34) \times 10^{-11}$ cm^3 molecule^{-1} s^{-1}. The cluster of points at [BrO] = 6.5×10^{12} molecule cm^{-3} were measured while varying [O_3] from (3.8 to 16.5) $\times 10^{14}$ molecule cm^{-3}.

TABLE 4: Experimental Parameters and Values of k_{1a}

T (K)	k_{1a}[b,c]	[BrO][b]	[O_3][b]	pressure[b]	velocity[b]
388	3.67 ± 0.60	4.48−23.9	5.6	6.8	900
369	4.34 ± 0.30	1.62−16.9	7.0	7.0	500
368	4.18 ± 0.22	3.44−21.1	5.6	7.0	900
329	5.46 ± 0.26	0.73−11.4	6.6	7.0	500
298	6.33 ± 0.34	2.15−15.9	3.3−8.1	6.6	500
298	6.07 ± 0.34	1.93−16.1	3.81−16.5	7.4	500
298	5.59 ± 0.40	3.01−15.7	22.0	6.6	900
298	6.22 ± 0.82	2.26−14.1	4.0	15.3	900
291[a]	6.13 ± 1.15	3.0−11.3	8.3	6.8	900
273	7.17 ± 0.41	1.82−12.5	4.2−5.3	7.4	500
252	8.15 ± 0.28	1.15−8.64	12.0−16.5	6.9	500
238	7.52 ± 0.82	2.06−10.6	20.0−22.6	6.9	500
222	8.64 ± 0.56	1.64−10.0	17.6	7.1	500
223	6.80 ± 1.26	1.18−9.12	16.5	6.7	900
222	7.21 ± 0.42	2.86−11.2	9.0	6.6	900
204	8.20 ± 0.78	1.67−10.0	14.0	7.0	500
204	7.02 ± 0.41	1.85−13.8	9.6	6.7	900
204	8.82 ± 0.50	2.59−11.9	8.0	6.7	900

[a] Differential cross section for 291 K was obtained by interpolating the data between 252 and 298 K. [b] BrO concentrations are in units of 10^{12} molecule cm^{-3}, O_3 concentrations are in 10^{14} molecule cm^{-3}, k_{1a} is in units of 10^{-11} cm^3 molecule^{-1} s^{-1}, velocity is in cm s^{-1}, and pressure is in Torr. [c] The uncertainty given for is 2σ from the fit and does not include the estimated uncertainty in [BrO] of 16%.

always within 3% of one another. Figure 5 shows a plot of k'_d versus [BrO] which yields k_{1a} (298 K) = $(6.05 \pm 0.57) \times 10^{-11}$ cm^3 molecule^{-1} s^{-1}. The quoted uncertainty is twice the standard deviation of the slope obtained from a weighted ($1/\sigma^2$) linear least-squares fit. The IO loss rate measured in the absence of BrO depended on the flow velocity and temperature and ranged from 170 to 350 s^{-1}. Varying the photolysis laser fluence {(0.1−0.75) mJ cm^{-2}} or [CF_3I] {(1.8−24) $\times 10^{14}$ molecule cm^{-3}} did not change the measured second-order rate coefficient. Varying the pressure between 6 and 15 Torr produced no significant change in the measured reaction rate coefficient. k_{1a} measured with flow velocities of 500 and 900 cm s^{-1}, at 6.6 Torr, were not significantly different. The cluster of points at [BrO] = 6.5×10^{12} molecule cm^{-3} were taken while varying [O_3] from (3.8 to 16.5) $\times 10^{14}$ molecule cm^{-3}. Measured rate coefficients for reaction 1a are summarized in Table 4. A fit of all the data to an Arrhenius expression yields $k_{1a}(T) = (2.5 \pm 1.0) \times 10^{-11} \exp[(260 \pm 100)/T]$ cm^3 molecule^{-1} s^{-1} and is shown in Figure 6, where the uncertainties

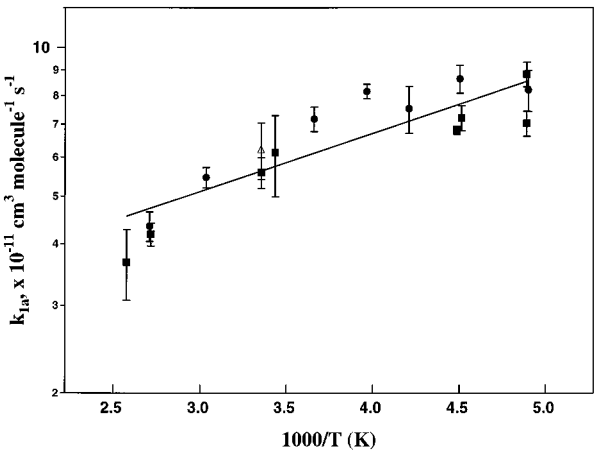

Figure 6. Plot of k_{1a} (log scale) vs 1000/T showing the temperature dependence of the total rate coefficient for reaction 1a measured in an excess of O_3. A fit to all of the data give an Arrhenius expression for $k_{1a}(T) = (2.5 \pm 1.0) \times 10^{-11} \exp[(260 \pm 100)/T]$ cm^3 molecule^{-1} s^{-1}. The quoted uncertainty is 2σ and includes 16% uncertainty in [BrO]. Data taken at 6−7 Torr with flow velocities of 500 cm s^{-1} (●) and 900 cm s^{-1} (■) and at 15.3 Torr with a flow velocity of 900 cm s^{-1} (△) are shown.

are 2σ and include estimated systematic errors. The Arrhenius plot is slightly curved and may indicate changes in the product branching ratios with temperature. The measured rate coefficients were independent of pressure, albeit over a small range. In the absence of any clear indications of a change in mechanism and because the measurements covered limited ranges of pressure and temperature, we have adopted the simple Arrhenius form. This should be sufficient for atmospheric applications because the temperature range of the measurements covers that found in the lower atmosphere.

Tests were performed to ensure that IO reactions with the BrO precursors did not interfere with our determination of k_{1a}. Reactions considered were

$$IO + Br_2 \rightarrow IBr + BrO \quad (14)$$

$$IO + O_3 \rightarrow I + 2O_2 \quad (15)$$

and

$$IO + Br \rightarrow BrO + I \quad (16)$$

By varying [Br_2] {(4−8) $\times 10^{14}$ molecule cm^{-3}} in the presence of IO, a limit for k_{14}(298 K) of $< 7 \times 10^{-14}$ cm^3 molecule^{-1} s^{-1} was obtained. Therefore, reaction 14 does not influence the IO temporal profile under our experimental conditions. k_{15} was not determined in the present study, but limits of $< 10^{-17}$ cm^3 molecule^{-1} s^{-1} for the ClO + O_3 and BrO + O_3 reactions[5] suggest that reaction 15 is slow. Recent experiments have shown that Br reacts rapidly with IO,[10,11] and its presence would limit our ability to measure k_1. To minimize reaction 16, k_{1a} was measured in excess O_3 ($> 3 \times 10^{14}$ molecule cm^{-3}). Br atoms, formed in the BrO self-reaction,[3] reacted with ozone {k_7(298 K) = 1.2×10^{-12} cm^3 molecule^{-1} s^{-1}} to reform BrO in our experiments. As shown in the Discussion, [Br] was small enough not to influence the measured value of k_{1a}.

The IO self-reaction

$$IO + IO \rightarrow \text{products} \quad (17)$$

is rapid, ($k_{17} \sim 1 \times 10^{-10}$ cm^3 molecule^{-1} s^{-1}), with a small I atom yield.[12] In the absence of BrO, varying [IO]$_0$ by a factor of 7 did not influence the measured loss rate of IO or change

TABLE 5: Recent Determinations of the BrO Self-Reaction Rate Coefficient

k_2 (298 K)[a]	scaled k_2[b]	k_{2a}/k_2	k_{2b}[c]	E/R (K)	A[a]	ref
3.4 ± 0.5				215 ± 50	1.70 ± 0.45	this work
2.98 ± 0.42	3.27	0.84	4.69 ± 0.68			Rowley *et al.*[16]
2.78 ± 0.25	3.06	0.85	3.9 ± 1.6			Mauldin *et al.*[3]
3.1 ± 0.4	3.4					Bridier *et al.*[15]
2.17 ± 0.68		0.84		225 ± 195	0.96	Sander *et al.*[14]
3.2 ± 0.5		0.85	4.7 ± 1.5			Lançar *et al.*[18]
3.2 ± 0.7						Clyne and Watson[19]
2.49 ± 0.26		0.88		251 ± 56	1.06 ± 0.20	Turnipseed *et al.*[17]
	3.25 ± 0.42			230 ± 100	1.50 ± 0.46	average[d]

[a] Units are 10^{-12} cm^3 molecule^{-1} s^{-1}. [b] These values have been scaled to cross sections measured in this experiment. [c] Units are 10^{-13} cm^3 molecule^{-1} s^{-1}. [d] For this average the UV measurements were scaled to the cross section determined here.

the shape of the IO temporal profile. Therefore, we determined that this reaction did not contribute to our observed IO loss.

Even in the presence of excess O_3, the BrO self-reaction (channel 2b) creates a concentration gradient along the length of the absorption cell. UV absorption measures a BrO column abundance which, when divided by the length of the cell, gives the average concentration of BrO. For the determination of k_{1a}, we needed to know [BrO] at the position where the IO temporal profile was probed. The column abundance is related to the [BrO] at the position where the IO temporal profile was monitored as shown in Appendix A. These calculations along with numerical simulations showed that when the IO temporal profile was monitored at the center of the absorption cell, the average [BrO] calculated from the column abundance was within 3% of that where the IO concentration is probed. In the worst case scenario, at 204 K under slow flow conditions (500 cm s^{-1}) with a initial BrO concentration ([BrO] = 1.4×10^{13} molecule cm^{-3}), this difference was still <5%. The factors that contribute to the uncertainty in [BrO] are path length 2%, temperature gradient <1%, and absorption cross section <10% and yield a total uncertainty in [BrO] of ∼16% at the 95% confidence level. This uncertainty has been included in the quoted uncertainty of k_{1a}.

Discussion

BrO Absorption Cross Sections. There is one previous study, from this laboratory, with which we can compare our results. Wahner *et al.*[13] measured the absolute cross section with spectral resolutions from 0.06 to 1.25 nm. Our 298 K value of 1.63×10^{-17} cm^2 molecule^{-1} for the (7,0) band is ∼10% larger than that measured by Wahner *et al.*,[13] 1.48×10^{-17} cm^2 molecule^{-1}, at the same resolution (0.5 nm). Although our absorption cross section at 298 K is larger than that of Wahner *et al.*,[13] the temperature dependence is the same. Sander and Watson[14] report a BrO absorption cross section of 1.14×10^{-17} cm^2 molecule^{-1} at a higher resolution, 0.09 nm. However, their measurements were shifted off of the peak of the (7,0) band, making a comparison between their measurement and ours difficult.

BrO + BrO Reaction Rate Coefficients. The BrO self-reaction has been studied by several groups. These studies can be broken down into those which used UV absorption[3,14−16] or mass spectrometry[17−19] for detecting BrO and are summarized in Table 5. The branching ratio, k_{2a}/k_2, is well established with a value of ∼0.85. However, the total rate coefficient is not as accurately known. It is important to note that depending upon the BrO source, some experiments measured only a branching ratio[15] or determined only k_2,[19] while others directly measured both the total rate coefficient and a branching ratio.[3,14,16−18] Our experiments, carried out in the absence of O_3, measured the total rate coefficient, k_2. Problems with formation of Br_2O have been reported in studies carried out in the presence of ozone.[3,15,16] Br_2O, if formed in our system, would quickly react with Br atoms to regenerate BrO. We cannot exclude the possibility of Br_2O_2 formation at low temperatures in our experiments, except to note that our second-order plots were linear at all temperatures.

In the experiments where BrO was detected by UV absorption, it is necessary to account for differences in BrO absorption cross sections used in the data analysis. Rowley *et al.*,[16] Mauldin *et al.*,[3] and Bridier *et al.*[15] detected BrO by UV absorption and used the cross sections of Wahner *et al.*[13] When their measured values of k_2 are scaled to our cross sections (Table 5), good agreement is obtained. To compare with the results of Sander *et al.*[14] we need to compare k_2/σ, and these values from the two studies agree within 12%. The k_2(298 K) measured in this experiment is in excellent agreement with that obtained by Lançar *et al.*[18] and Clyne and Watson.[19] However, it is ∼30% larger than the value obtained by Turnipseed *et al.*[17] who also used mass spectrometric detection. The reason for this discrepancy is unknown.

The temperature dependence of the BrO self-reaction measured in this laboratory, along with those of Turnipseed *et al.*,[17] Sander *et al.*,[14] and Mauldin *et al.*,[3] are shown in Figure 3. We have excluded one data point of Turnipseed *et al.*[17] and have scaled the data of Mauldin *et al.*[3] to our cross sections. The two previously reported values for E/R, (225 ± 195) K[14] and (251 ± 56) K,[17] are in excellent agreement with the value of (215 ± 50) K obtained here. An average E/R of (230 ± 100) K appears to be suitable for atmospheric modeling. Our recommended value for atmospheric modeling is $k_2(T) = (1.50 \pm 0.46) \times 10^{-12} \exp[(230 \pm 100)/T]$ cm^3 molecule^{-1} s^{-1}. The preexponential factor given is a weighted average of the data from all studies.

IO + BrO Reaction Rate Coefficients. There are numerous potential sources of error in measuring the rate coefficient for reaction 1. Reaction 1 involves two reactive species, and, despite great care, other reactive species are present in our system and could influence either the temporal profile of IO or the concentration of BrO. The BrO self-reaction, which produced a concentration gradient along the length of the reactor, was explicitly taken into account; this loss resulted in an uncertainty in the measured value of k_{1a} by at most 10%. Other sources of error are (1) the IO self-reaction (discussed in the Results), (2) production of Br atoms and their subsequent reactions with IO, and (3) wall loss of BrO.

We did not directly detect Br atoms in this system. To assess their impact on measured values of k_{1a}, we estimated their concentrations and their influence on IO temporal profiles via numerical simulations.[20] Temporal profiles of BrO and Br in the cell were simulated using the reactions listed in Table 6. The concentrations of Br at various positions along the reactor were calculated for different [BrO] {(1−14) × 10^{12} molecule cm^{-3}} and [O_3] {(10^{13}−10^{15}) molecule cm^{-3}} at several

TABLE 6: Reaction Mechanism Used To Estimate [BrO] and [Br] along the Reaction Cell

reaction	$k(T)$	notes
$BrO + BrO \rightarrow Br_2 + O_2$	$4.1 \times 10^{-14} \exp[660/T]^a$	$[BrO]_0$ fixed[b] $(1-14) \times 10^{12}$
$BrO + BrO \rightarrow 2\,Br + O_2$	$4.0 \times 10^{-12} \exp[-190/T]^a$	$[BrO]_0$ fixed[b] $(1-14) \times 10^{12}$
$Br + O_3 \rightarrow BrO + O_2$	$1.7 \times 10^{-11} \exp[-800/T]^a$	*b*
$BrO \rightarrow$ loss	$\leq 6\ s^{-1}$	*c*
$Br \rightarrow$ loss	$\leq 6\ s^{-1}$	*d*

[a] Units for $k(T)$ are cm^3 molecule^{-1} s^{-1}; values for $k(T)$ are from ref 5. [b] At each BrO concentration in this range a simulation at 3−5 different $[O_3]$ was done to determine [BrO]/[Br]. BrO concentrations are in units of molecule cm^{-3}. [c] An upper limit determined from the wall loss experiments described in the text. [d] Assumed to be the same as the BrO wall loss.

temperatures. From these we estimated that in order to maintain [BrO]/[Br] > 10, $[O_3] > 3 \times 10^{14}$ molecule cm^{-3} was required at 298 K; at lower temperatures, still higher $[O_3]$ ($>7 \times 10^{14}$ molecule cm^{-3}) was necessary. The concentrations of BrO and Br at various positions in the reactor were calculated for each set of experimental conditions in Table 4. At the ozone concentrations used in these experiments, the [BrO]/[Br] ratio was always >10, and for most experiments, it was >20. In addition, any iodine atoms produced in the reaction of IO with Br would be recycled by O_3 back to IO.

First-order wall loss of BrO radicals is expected to be small[19] and therefore should not influence our measurements. The BrO wall loss was tested by varying the flow velocity through the reactor from 500 to 900 cm s^{-1}. As shown in Table 4, the measured values of k_{1a} were insensitive to this change. According to the numerical simulations, a BrO wall loss coefficient of $\leq 6\ s^{-1}$ would alter the measured rate coefficient by <10%.

Products of the IO + BrO Reaction. Since our experiments were insensitive to channels producing atomic iodine, we have broken down product channels into those which do not directly produce iodine atoms

$$BrO + IO \rightarrow IBr + O_2 \qquad (1a_1)$$

$$\rightarrow Br + OIO \qquad (1a_2)$$

$$\rightarrow Br + IOO \qquad (1a_3)$$

$$\rightarrow IBrO_2 \qquad (1a_4)$$

and those which do

$$BrO + IO \rightarrow I + Br + O_2 \qquad (1b_1)$$

$$\rightarrow I + BrOO \qquad (1b_2)$$

$$\rightarrow I + OBrO \qquad (1b_3)$$

Since the thermochemistry for many of the products is unknown, it cannot be used to constrain the possible pathways.

The branching ratio for channels producing atomic iodine (1b) was estimated at 298 K by measuring the temporal profiles of IO in an excess of BrO while varying $[O_3]$ from (3.8 to 16.5) $\times 10^{14}$ molecule cm^{-3} (Figure 7). At a given initial [BrO], increasing the ozone concentration increases the rate of regeneration of IO and BrO via reactions 7 and 13. Formation of atomic iodine as a reaction product would be evident in the changes in the IO temporal profile with increasing $[O_3]$. The temporal profiles of IO were then modeled using Facsimile[20] with the reactions given in Table 7. Numerical simulations of the IO temporal profiles, Figures 6 and 8, showed that I atom production was ≤35%.

We have measured the rate coefficient for reaction 1a, the sum of non-iodine atom producing channels. On the basis of the upper limit of 35% for the I atom producing channels, we can place an upper limit for $k_1(298)$, the total rate coefficient ($k_{1a} + k_{1b}$), of 1.0×10^{-10} cm^3 molecule^{-1} s^{-1}. Further, the measured k_{1a} is a lower limit for $k_1(298)$ of 6.0×10^{-11} cm^3 molecule^{-1} s^{-1}. Since this work was initiated, Laszlo *et al.*[21] have measured k_1 from the photolysis of $Br_2/I_2/N_2O$ or IBr/N_2O mixtures. By simultaneously measuring the transient absorption of BrO and IO and fitting the observed decays with a reaction mechanism, they obtained a value of $k_1(298\ K) = (6.9 \pm 2.7) \times 10^{-11}$ cm^3 molecule^{-1} s^{-1}. Their 298 K value is in agreement with our results: however, their measurements were limited to 298 K, and a comparison of the temperature dependence is not possible. The branching ratios for various channels are still unclear and need to be explored.

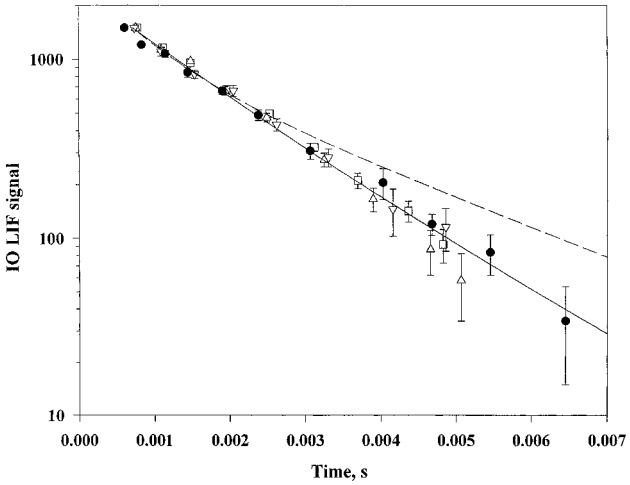

Figure 7. IO temporal profiles measured with [BrO] = 8.7×10^{12} molecule cm^{-3} and $[O_3] = 5 \times 10^{14}$ molecule cm^{-3} (●), $[O_3] = 7.3 \times 10^{14}$ molecule cm^{-3} (○), $[O_3] = 12 \times 10^{14}$ molecule cm^{-3} (▽), and $[O_3] = 16.5 \times 10^{14}$ molecule cm^{-3} (△). The solid line is the numerical simulation of the data obtained with $[O_3] = 5 \times 10^{14}$ molecule cm^{-3} (●) and $k_{1b} = 0$. The dashed line is a simulation with $k_{1b} = 3.2 \times 10^{-11}$ cm^3 molecule^{-1} s^{-1}, or an iodine atom yield of 35%.

TABLE 7: Reaction Mechanism Used To Estimate I Atom Channel for Reaction 1 at 298 K

reaction	k^a	notes
$BrO + BrO \rightarrow Br_2 + O_2$	3.8×10^{-13}	$[BrO]_0$[b] fixed at 8.7×10^{12}
$BrO + BrO \rightarrow 2\,Br + O_2$	2.1×10^{-12}	
$Br + O_3 \rightarrow BrO + O_2$	1.2×10^{-12}	[Br] calculated
$BrO \rightarrow$ loss	$4-6\ s^{-1}$	*c*
$Br \rightarrow$ loss	$4-6\ s^{-1}$	c
$BrO + IO \rightarrow I + Br + O_2$	$(0-3.2) \times 10^{-11}$	varied
$BrO + IO \rightarrow$ products	6.0×10^{-11}	measured
$I + O_3 \rightarrow IO + O_2$	1.3×10^{-12}	
$IO \rightarrow$ loss	$185\ s^{-1}$	measured[d]

[a] Rate coefficients are in units of cm^3 molecule^{-1} s^{-1}, unless otherwise noted. Rate coefficients are all from DeMore *et al.*,[5] unless otherwise noted. [b] Concentrations are in molecule cm^{-3}. [c] Calculated as described in text. [d] Measured in the absence of BrO.

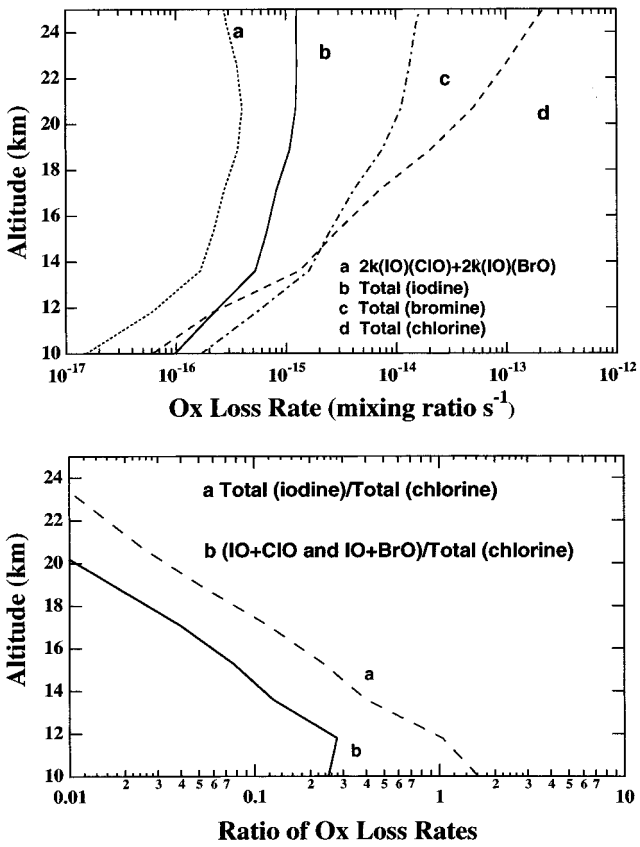

Figure 8. (Top) Calculated rate of odd oxygen destruction for midlatitudes in spring from various halogens for 1990 conditions using an iodine mixing ratio of 0.5 pptv: (a) the contribution due to the interhalogen reactions IO + ClO and IO + BrO, (b) the contribution from all iodine reactions; (c) the values due to bromine chemistry; (d) the calculated rate due to chlorine chemistry. The contributions from the ClO−BrO catalytic cycle are included in both (c) and (d). (Bottom) (a) the relative contributions of all iodine reactions; (b) the interhalogen iodine reactions, relative to the chlorine-related in-situ chemical loss.

Atmospheric Implications

In this section, we will illustrate that even rather small stratospheric iodine abundances could contribute to the observed midlatitude lowermost stratospheric ozone depletion. A complete review of midlatitude ozone loss is beyond the scope of this paper. Therefore, we will limit our discussion to the impact of iodine chemistry through the use of the model described in detail by Solomon *et al.*[22] and references therein, with the inclusion of the rate coefficients reported here. Volcanic aerosols were held constant in these calculations, and we examine the ozone trends and budgets for this evaluation.

The possible influence of iodine chemistry on ozone trends depends upon several factors: (i) the rate coefficients for the reactions of IO with ClO, BrO, and HO_2, the rate-limiting steps in catalytic cycles leading to ozone destruction, (ii) the branching ratios for the reaction channels that lead to ozone destruction, (iii) the partitioning of IO in the atmosphere, and (iv) the abundance and any trends in atmospheric IO.

The abundance and trends of stratospheric iodine are poorly known. Observations of methyl iodide in the tropical upper troposphere by Davis *et al.*[23] suggest an input of methyl iodide alone to the tropical stratosphere of the order (0.5−0.66) pptv. However, visible spectroscopic studies by Wennberg *et al.*[24] and Pundt *et al.*[25] suggest upper limits to twilight IO abundance of at most about half of these values. We adopt a total iodine mixing ratio in the tropical stratosphere of 0.5 pptv, as suggested by Davis *et al.*[23] This leads to a calculated noon midlatitude abundance of IO of (0.1−0.3) pptv from (12 to 20) km. This is close to the upper limits reported by Wennberg *et al.*[24] and Pundt *et al.*[25]

The results of the model calculations are shown in Figure 8. Figure 8 shows the odd oxygen loss rates due to chlorine, bromine, and iodine chemistry calculated in the model for 1990 spring conditions. Much of the total calculated lower stratospheric iodine loss rate is due to the reaction of IO with HO_2. The IO + ClO reaction makes only a small contribution to the total loss rate because the rate coefficient is a factor of 5 slower than that used in the earlier model calculation.[22] However, the IO + BrO reaction makes a significant contribution with the caveat that the products of this reaction lead to ozone loss. Our present understanding suggests that IO chemistry contributes to the observed midlatitude ozone trends below 20 km unless its abundance is considerably less than 0.1 pptv.

The importance of local chemistry compared to transport from other regions (such as the Arctic) is a key and presently uncertain factor determining the role of iodine relative to other halogens in ozone depletion at midlatitudes. While the primary source of iodine is believed to be natural (from biological processes in the ocean), the possibility of trends cannot be ruled out (related for example, to changing sea surface temperatures). A trend is an interesting and important factor in the ozone budget both for the stratosphere and upper troposphere. If we were to assume a trend of 0.5 pptv over the past decade, our model predicts that it would directly increase the calculated ozone losses in the lowermost midlatitude stratosphere by 50%.

In conclusion, the observed ozone depletion at midlatitudes in the lowermost stratosphere remains considerably greater than that calculated with our model. Therefore, the modeling of ozone depletion at midlatitudes remains incomplete even when iodine chemistry is considered. The rate coefficients reported here could be used to model the episodic Arctic ozone depletion if the concentrations of BrO and IO are measured.

Acknowledgment. This work was funded in part by NASA's Mission to Planet Earth Program through the Upper Atmospheric Research Program.

Appendix A

The BrO column abundance, C_{BrO} (molecule cm^{-2}), is given by the integral of the concentration of BrO along the column length (z),

$$C_{BrO} = \int_0^z [BrO]_t \, dz$$

where $z = tv$, v is the average flow velocity, and t is the reaction time with zero being the entrance of the absorption cell. The concentration of BrO as a function of time ($[BrO]_t$) is given by eq III (where k_2 has been replaced by k_{2a} since these experiments were done in excess ozone)

$$[BrO]_t = \frac{[BrO]_0}{1 + 2k_{2a}t[BrO]_0}$$

which leads to

$$C_{BrO} = \int_0^z \frac{[BrO]_0}{1 + 2k_{2a}z/v[BrO]_0} \, dz$$

The solution to this expression is

$$C_{\mathrm{BrO}} = \frac{v}{2k_{2a}} \ln\left(1 + \frac{2k_{2a}z}{v}[\mathrm{BrO}]_0\right)$$

$[BrO]_0$ can be calculated from the measured C_{BrO} by knowing the average flow velocity and the length of the absorption cell. Further, from $[BrO]_0$ and the time to reach the probe position, $[BrO]_t$ at the probe position can be calculated from eq III. Since we measured k_1 in an excess of ozone, Br atoms produced by reaction 2b were recycled and reaction 2a is the major loss process for BrO (in the absence of IO). The average concentration $\langle[BrO]\rangle$ is given by C_{BrO}/z and was within 3% of the calculated value of $[BrO]_t$.

References and Notes

(1) Turnipseed, A. A.; Gilles, M. K.; Burkholder, J. B.; Ravishankara, A. R. *J. Phys. Chem. A* **1997**, *101*, 5517.
(2) Sturges, W. T., Barrie, L. A. *Atmos. Environ.* **1988**, *22*, 1179.
(3) Mauldin, R. L., III; Wahner, A.; Ravishankara, A. R. *J. Phys. Chem.* **1993**, *97*, 7585.
(4) Yokelson, R. J.; Burkholder, J. B.; Goldfarb, L.; Fox, R. W.; Gilles, M. K.; Ravishankara, A. R. *J. Phys. Chem.* **1995**, *99*, 13976.
(5) DeMore, W. B.; Sander, S. P.; Golden, D. M.; Hampson, R. F.; Kurylo, M. J.; Howard, C. J.; Ravishankara, A. R.; Kolb, C. E.; Molina, M. J. *Chemical Kinetics and Photochemical Data for Use in Stratospheric Modeling, Evaluation No. 11*; Jet Propulsion Laboratory: Pasadena, CA, 1994.
(6) Nicovich, J. M.; Wine, P. H. *Int. J. Chem. Kinet.* **1990**, *22*, 379.
(7) Turnipseed, A. A.; Gilles, M. K.; Burkholder, J. B.; Ravishankara, A. R. *Chem. Phys. Lett.* **1995**, *242*, 427.
(8) Gilles, M. K.; Turnipseed, A. A.; Talukdar, R. K.; Rudich, Y.; Villalta, P. W.; Huey, L. G.; Burkholder, J. B.; Ravishankara, A. R. *J. Phys. Chem.* **1996**, *100*, 14005.
(9) Atkinson, R.; Baulch, D. L.; Cox, R. A.; Hampson, R. F.; Kerr, J. A.; Troe, J. *J. Phys. Chem. Ref. Data* **1992**, *21*, 1125.
(10) Gilles, M. K.; Turnipseed, A. A.; Burkholder, J. B.; Ravishankara, A. R. *Chem. Phys. Lett*., in press.
(11) Bedjanian, Y.; LeBras, G.; Poulet, G. *Chem. Phys. Lett.* **1997**, *266*, 233.
(12) Harwood, M. H.; Burkholder, J. B.; Hunter, M.; Fox, R. W.; Ravishankara, A. R. *J. Phys. Chem. A* **1997**, *101*, 853.
(13) Wahner, A.; Ravishankara, A. R.; Sander, S. P.; Friedl, R. R. *Chem. Phys. Lett.* **1988**, *152*, 507.
(14) Sander, S. P., Watson, R. T. *J. Phys. Chem.* **1981**, *85*, 4000.
(15) Bridier, I.; Veyret, B., Lesclaux, R. *Chem. Phys. Lett.* **1993**, *201*, 563.
(16) Rowley, D. M.; Harwood, M. H.; Freshwater, R. A., Jones, R. L. *J. Phys. Chem.* **1996**, *100*, 3020.
(17) Turnipseed, A. A.; Birks, J. W.; Calvert, J. G. *J. Phys. Chem.* **1990**, *94*, 7477.
(18) Lançar, I.; Laverdet, G.; LeBras, G.; Poulet, G. *Int. J. Chem. Kinet.* **1991**, *23*, 37.
(19) Clyne, M. A. A.; Watson, R. T. *J. Chem. Soc., Faraday Trans. I* **1975**, *71*, 336.
(20) Malleson, A. M.; Kellett, H. M.; Myhill, R. G., Sweetenham, W. P. *FACSIMILE*; A. E. R. E. Harwell Publications Office: Oxfordshire, 1990.
(21) Laszlo, B.; Huie, R. E.; Kurylo, M. J., Miziolek, A. W. *J. Geophys. Res.* **1997**, *102*, 1523.
(22) Solomon, S.; Garcia, R. R., Ravishankara, A. R. *J. Geophys. Res.* **1994**, *99*, 20491.
(23) Davis, D.; Crawford, J.; Liu, S.; McKeen, S.; Bandy, A.; Thornton, D.; Rowland, F.; Blake, D. *J. Geophys. Res.* **1996**, *101*, 2135.
(24) Wennberg, P. O.; Brault, J. W.; Hanisco, T. F.; Salawitch, R. J.; Mount, G. H. *J. Geophys. Res.* **1997**, *102*, 8887.
(25) Pundt, I.; Pommereau, J. P.; Phillips, C.; Lateltin, E. *J. Atmos. Chem.*, in press.
(26) Solomon, S.; Burkholder, J. B.; Ravishankara, A. R.; Garcia, R. R. *J. Geophys. Res.* **1994**, *99*, 20929.
(27) Molina, L. T.; Molina, M. J. *J. Geophys. Res.* **1986**, *91*, 14501.
(28) Gibson, G. E.; Bayliss, N. S. *Phys. Rev.* **1933**, *44*, 188.